The thalamus regulates retinoic acid signaling and development of parvalbumin interneurons in postnatal mouse prefrontal cortex

Rachel Larsen*, Alatheia Proue*, Matthew Christiansen, Yasushi Nakagawa#

Department of Neuroscience, University of Minnesota Medical School

*These authors eually contributed to the work.

#Corresponding author:

Yasushi Nakagawa, M.D., Ph.D.

Department of Neuroscience, University of Minnesota Medical School

6-145 Jackson Hall, 321 Church Street SE

Minneapolis, MN 55455

e-mail: nakagawa@umn.edu

Number of figures: 8

Number of supplemental figures: 5

Number of tables: 0

Abstract

GABAergic inhibitory neurons in the prefrontal cortex (PFC) play a crucial role in higher cognitive functions. Although disruption of their normal development is linked to a number of psychiatric disorders, cellular and molecular mechanisms underlying the normal development of these neurons are poorly understood. Here we found that during postnatal mouse development, *Cyp26b1*, a gene encoding a retinoic acid-degrading enzyme, is strongly expressed in the PFC and that medial ganglionic eminence (MGE)-derived interneurons are the main cell population that respond to retinoic acid. Mice lacking *Cyp26b1* in the PFC had an increased density of parvalbumin (PV)-expressing, but not somatostatin-expressing, interneurons. Furthermore, initiation of *Cyp26b1* expression in layer 6 cells in neonatal PFC required the connections between the thalamus and PFC but not transmitter release from thalamocortical axons, indicating that the thalamus plays a novel, essential role in regulating postnatal development of PV neurons in the PFC by inducing the expression of *Cyp26b1*. Together with the finding that MGE-derived interneurons depend on the thalamus for their radial positioning within the embryonic cortical plate throughout the neocortex, our results show that the thalamus regulates the development of PFC interneurons both by cortex-wide and area-specific mechanisms.

Keywords

prefrontal cortex, interneurons, parvalbumin, retionic acid, CYP26B1, thalamus, thalamocortical axons

Introduction

The prefrontal cortex (PFC) plays a crucial role in higher brain functions. It has connections with several brain regions including the thalamus, amygdala, hippocampus and striatum, and integrates many modalities of information for goal-oriented behaviors and emotion. Aberrant development of the PFC has been linked to many brain disorders including schizophrenia, autism spectrum disorders, attention deficit hyperactivity disorders (ADHD), depression and bipolar disorders[1]. More specifically, developmental trajectories of GABAergic interneurons, particularly those expressing the calcium-binding protein parvalbumin (PV), are impaired in both human patients and animal models of these disorders[2–7]. Therefore, determining the normal developmental mechanisms of PFC interneurons is likely to provide important insights into the pathogenesis and treatment of these disorders.

Development of cortical interneurons is regulated by both intrinsic and extrinsic mechanisms[8,9]. One key extrinsic cue is the input from the thalamus, which regulates migration and maturation of cortical interneurons both prenatally and postnatally in mice [10–13]. However, most studies addressing the role of thalamic input in interneuron development have been performed on primary visual or somatosensory cortex, while little is known about the mechanisms specific to the PFC. The protracted maturation of PFC interneurons compared with other cortical areas[14–16] and the distinct set of thalamic nuclei that are connected to the PFC[17,18] suggest the presence of extrinsic regulatory mechanisms for interneuron development unique to the PFC.

One candidate molecule that may play a role in postnatal development of the PFC is retinoic acid (RA), a derivative of vitamin A. RA is critical for many important

aspects of brain development, ranging from rostrocaudal patterning of hindbrain and spinal cord to synaptic plasticity[19–23]. *Cyp26b1*, which encodes a crucial RA-degrading enzyme[24–26], is expressed in the deep layer of the frontal cortex (Allen Brain Atlas), and *Aldh1a3*, which encodes an RA-synthesizing enzyme, is transiently expressed in the superficial layer of the medial PFC during postnatal development[27]. Therefore, the balance between production and degradation of RA might play an unexplored role in postnatal development of medial PFC.

In this study, we first demonstrated that in medial PFC, *Cyp26b1* is transiently expressed in layer 6 cells from postnatal day 2 (P2) to P21, and that a subpopulation of PV interneurons are the main cell type that responds to RA. These results led us to hypothesize that RA signaling regulated by *Cyp26b1* plays a region-specific role in controlling interneuron development in the PFC. In fact, we found that frontal cortex-specific *Cyp26b1* mutant mice had an increased density of PV-expressing neurons in medial PFC at P14 and P21. We also found that postnatal expression of *Cyp26b1* in medial PFC was dependent on the connections between the thalamus and PFC. Additionally, thalamocortical projections were required for normal radial allocation of PFC interneurons during embryogenesis. These results demonstrate that the thalamus plays multiple crucial roles in interneuron development in the PFC first by controlling their positioning during embryonic stages and then by restricting the maturation of PV neurons by inducing a retinoic acid-degrading enzyme.

Results

Cyp26b1, a gene encoding a retinoic acid degrading enzyme, is expressed in a spatially and temporally dynamic pattern in the mouse PFC

In order to identify genes that are enriched in developing PFC, we screened the Anatomic Gene Expression Atlas (AGEA)[41]. The database showed that *Cyp26b1*, a gene that encodes a retinoic acid (RA)-degrading enzyme, is strongly expressed in the frontal cortex at postnatal day 14 (P14), including the deep layer of medial and ventral PFC as well as the middle layer of lateral cortex extending into the agranular insula. We therefore examined the developmental expression patterns of *Cyp26b1* in more detail by in situ hybridization. Strong expression of *Cyp26b1* was observed in the medial PFC starting at P2 (Fig.1A). Comparison with the layer 6 marker, *Synaptotagmin 6 (Syt6)*, showed that *Cyp26b1* is expressed in layer 6 of medial and ventral PFC (compare Fig. 1B and D). In addition to being spatially restricted, expression of *Cyp26b1* was also temporally dynamic; it was strong in medial PFC until P14 (Fig.5C), and by P21, the medial expression was much weaker compared with ventral and lateral regions (Fig. 1E). By P35, there was no detacable expression of *Cyp26b1* in medial PFC, yet the expression persisted in ventral and lateral frontal cortex (Fig.1F).

The tissue RA level is controlled both by its synthesis from vitamin A and by its degradation by CYP26 enzymes. Members of the aldehyde dehydrogenase 1 family are crucial synthesizing emzymes of RA, and two members of this family (ALDH1A2 and ALDH1A3) are expressed in early postnatal cortex; *Aldh1a2* is broadly expressed in the meninges [42], whereas *Aldh1a3* was specifically expressed in layer 2 of postatal medial PFC (Fig.1C;[27,42]). The expression of *Aldh1a3* in medial PFC starts at P0 and peaks by

P6[27], and becomes undetectable by the adult stage (data not shown). Outside of the frontal cortex, we detected no expression of *Cyp26b1* in more caudal parts of the neocortex including sensory areas at any of developmental stages that we examined (Fig.S1D,E). *Cyp26b1* was also expressed in the piriform cortex, amygdala, CA3 and hilus regions of the hippocampus and globus pallidus (Fig.S1C,E). Expression in these regions continues into adulthood (Allen Brain Atlas).

In summary, in the medial part of early postnatal PFC, RA is produced by cells in the superficial region, whereas CYP26B1, an RA degrading enzyme or an “RA sink”, is located in layer 6. Expression of both *Aldh1a3* and *Cyp26b1* was transient (summarized in Fig.1G). These results suggest that RA signaling is spatially and temprolly controlled and this regulation might play a role in the development of medial PFC.

Pavalbumin-expressing interneurons in medial PFC respond to retinoic acid during early postnatal development

The spatiotemporal expression pattern of *Cyp26b1* prompted us to explore the cellular tagets of RA signaling during PFC development. In order to determine the populations of cells that respond to RA, we analyzed the *RARE-LacZ* transgene, which reports the transcriptional activity of RAR/RXR heterodimers as RA receptors[28]. At P0, expression of β-galactosidase (β-gal) was barely detectable in medial PFC except in radial glial fibers (Fig.2A). At P8, a small number of β-gal-positive cells were detected. Most of these cells were in layer 5 (Fig.2L) and were also positive for SOX6, a marker for GABAergic interneurons derived from medial ganglionic eminence (MGE) [43] (Fig. 2B). This was still the case at P14 (Fig.2F-H); analysis of three transgenic brains

revealed that 91% of β-gal-positive cells in layer 5 were also SOX6-positive (Fig.2M). Markers of other neuronal types, including SP8 (Fig.2C,I; caudal ganglionic eminence (CGE)-derived cortical interneurons)[44], CTIP2 (Fig.3D,J; layer 5 subcerebral projection neurons as well as some interneurons)[45–47] and TBR1 (Fig.2E,K; layer 6 corticothalamic projection neurons) did not overlap with β-gal, indicating that these types of neurons do not express necessary molecular machineary to respond to RA via RAR/RXR heterodimers. In summary, within early postnatal medial PFC, the main populations of RA responding cells were MGE-derived interneurons.

Most MGE-derived interneurons in the adult neocortex express either somatostatin (SST) or parvalbumin (PV)[48,49]. A majority of these interneurons complete their tagential migration into the neocortex by birth[50,51]. Expression of PV protein or *Pvalb* mRNA is a hallmark of maturation of cells in the PV interneuron lineage. At P8, cells expressing PV protein or *Pvalb* mRNA were not detected in medial PFC (Fig.3A arrow; Fig3D), whereas these cells were already abundant in the lateral portion of the neocortex including motor and sensory areas (Fig.3A, double arrows). Thus, maturation of PV neurons is protracted in the PFC. By P14, *Pvalb* mRNA and PV protein were detected in medial PFC, mainly in layer 5 (Fig.3B, arrow; Fig3F,G).

In order to determine if RA-responding cells are restricted to either PV or SST neurons, we analyzed the medial PFC of *RARE-LacZ* transgenic mice for co-localization of β-gal and PV as well as β-gal and SST (Fig.3F,G). A strong overlap was observed between PV and β-gal (Fig.3F,F'). In three P14 brains, 48% percent of β-gal-positive cells in layer 5 were also PV positive (Fig.3H). In turn, 45% of PV positive cells in layer 5 were also β-gal-positive (Fig.3I). In sharp contrast, SST did not show any overlap with

β-gal from P8 through P67 (Fig.3E and data not shown). These results suggest that most of the overlap between SOX6 and β-gal is accounted for by RA-responding PV neurons (summarized in Fig.3J).

Cyp26b1 **is required for normal development of parvalbumin-expressing interneurons in medial PFC**

Because of the strong corelation between PV expression and response to RA, we hypothesized that development of PV interneurons in medial PFC is regulated by RA signaling and that this regulation depends on CYP26B1. To test this, we generated conditional *Cyp26b1* mutant mice in whcih *Cyp26b1* is deleted in the PFC. Because the expression of *Cyp26b1* is highly specific to layer 6 in medial PFC, we used *Synaptotagmin-6 Cre* (*Syt6-Cre*) driver mice[29,30]. *Syt6* expression is specific to layer 6 in the neocortex (Fig.1D), and *Syt6-Cre* mice allow recombination in layer 6 corticothalamic projection neurons in the frontal cortex including the medial PFC (Allen Brain Atlas; http://connectivity.brain-map.org/). In *Syt6-Cre/+*; *Cyp26b1*$^{flox/flox}$ (*Cyp26b1 CKO*) mice, *Cyp26b1* mRNA was not detected in medial PFC (Fig.S3C,D), whereas expression in other brain regions including the hippocampus and agranular insular cortex was not affected (Fig.S3C-F), comfirming an efficient and specific deletion of *Cyp26b1*.

We then counted the number of *Pvalb* mRNA-expressing neurons and compared the numbers between *Cyp26b1* CKO mice and their littermate controls at P14 and P21. At both stages, the density of *Pvalb*-positive cells was significantly increased in medial PFC of *Cyp26b1* mutant mice (Fig.4). When the PFC was divided into superficial and

the deep layers, the difference was seen only in the deeper half of the medial PFC, consistent with the distribution of β-gal expressing cells. A similar pattern was observed for PV protein at P14 (data not shown). In contrast, the number of *Sst*-expressing or *Vip*-expressing neurons (cells derived from caudal ganglionic eminence) was not significantly different in *Cyp26b1* mutant mice compared with controls (Fig.S3A-F). These results show that transient expression of *Cyp26b1* in medial PFC is specifically required for controlling the development of PV interneurons.

***Cyp26b1* is not expressed in medial PFC in the absence of thalamus-PFC connectivity**

Because *Cyp26b1* starts to be expressed in medial and ventral PFC when the reciprocal connections with the thalamus are being established, we next determined if normal expression of *Cyp26b1* depends on this connectivity. In our previous study, thalamus-specific deletion of the homeobox gene *Gbx2* resulted in severe deficiency of thalamocortical and corticothalamic projections in sensory areas (Vue et al., 2013). In order to determine if the same mice are deficient in thalamus-PFC connections, we examined the localization of NetrinG1 immunoreactivity[33,52] in thalamocortical axons (Fig.S4). Similar to the more caudal part of the cortex, the PFC of *Gbx2* cko mice showed a significant reduction in NetrinG1 staining at E16.5 (Fig.S4A,B). Quantitative measurement indicates that the overall fluorescent intensity of NetrinG1 staining was approximately 10% of the control case (data not shown). To test if the defect persists into postnatal stages, we placed DiI crystals in the medial PFC of fixed P14 brains of *Gbx2* mutants and wild type littermates. Both retrograde labeling of thalamic neurons

and anterograde labeling of corticothalamic axons (Fig.S4C,D) were serverely attenuated in *Gbx2* mutants. These results demonstrate a robust reduction of reciprocal connectivity between the thalamus and PFC in *Gbx2* mutant mice.

We then used *Gbx2* mutant mice to determine the requirement of thalamus-PFC connections in the normal expression of *Cyp26b1* in medial PFC. Already at P2, *Gbx2* mutant cortex lacked the expression of *Cyp26b1* in medial and ventral PFC (Fig.5A,B), demonstrating a requirement of thalamocortical interactions for the onset of *Cyp26b1* expression. The deficiency of *Cyp26b1* in the medial and ventral PFC in *Gbx2* mutant mice continued until P21, when the medial PFC expression of *Cyp26b1* normally started to decline (Fig.5D,I). In contrast, expression of *Cyp26b1* showed no alterations in lateral frontal cortex including the motor areas as well as agranular insular region (Fig.5). Other forebrain regions that normally express *Cyp26b1* were also unaffected (data not shown). The layer 6 marker, *Syt6* was still highly expressed in the frontal cortex of *Gbx2* mutants (Fig.5K,N), making it unlikely that the lack of *Cyp26b1* is due to the lack of layer 6 cells in *Gbx2* mutants. Lastly, *Aldh1a3*, which encodes an RA-syntheizing enzyme, shows a transient pattern of expression in postnatal PFC[27], similar to *Cyp26b1*. However, its expression was qualitatively unaffected in *Gbx2* mutant mice (Fig.5L,O). In summary, transient expression of *Cyp26b1* in layer 6 of medial PFC was dependent on the connections between the thalamus and the cortex (summarized in Fig.5M,P). Putting together the role of *Cyp26b1* in the development of PV neurons in medial PFC, our results collectively demonstrate a novel, indirect role of the thalamus in regulating the neocortical interneuron development.

Lack of thalamus-PFC connectivity results in early aberrancy in radial positioning of MGE-derived interneurons

Recent sutdies have unveiled a variety of celluar and molecular mechanisms by which the thalamocortical afferents affect the development of interneurons in primary somatosensory and visual cortex[10–13]. To determine the net outcome of the lack of interactions between the thalamus and the PFC, we examined the densities of *Pvalb*- and *Sst*- expressing interneurons in *Gbx2* mutant mice at P21. We found that both populations of interneurons were reduced in the middle layers of the medial PFC of *Gbx2* mutants (Fig.6A-C). These changes were broader than what we observed in *Cyp26b1* mutant mice, in which only PV neurons were increased. Therefore, within the developing medial PFC, the thalamus plays multiple roles in development of interneurons, some of which are independent of *Cyp26b1* expression. Indeed, already at P0 before *Cyp26b1* is normally expressed, we observed a significant reduction of LHX6-expressing, MGE-derived interneurons in the middle layer of medial PFC (Fig.6D-F). In contrast, the number in layer 6 or below was increased compared with the control (Fig.6F). Because the total number of LHX6-expressing cells remained unchanged in *Gbx2* mutants (Fig.6G), the reciprocal changes between the middle and deep layers indicate the impairment of radial distribution of MGE-derived interneurons with normal tangenital migration. This early phenotype is remarkably similar to a recent findng in sensory and motor cortex of thalamus-specific *Gbx2* as well as *vGluT2* mutant mice[10], demonstrating that this early, likley glutamate-dependent mechanism that regulate radial positioning of interneurons applies throughout the neocortex.

Induction of *Cyp26b1* by the thalamus is independent of transmitter release from thalamocortical projection neurons

In order to explore the mechanisms by which the thalamus controls the expression of *Cyp26b1* in the medial PFC, we next determined if blocking transmitter release from thalamocortical axon terminals recapitulates the phenotype in *Gbx2* mutant mice. For this purpose, we generated mice in which tetanus toxin light chain (TeNT) is ectopically expressed specifically in thalamocortical projection neurons (Fig.7). In TeNT-expressing mice at E16.5, expression of VAMP2, the target of TeNT, is dramatically reduced in thalamocortical axons, while it was retained in corticofugal axons (Fig.7A-D). At P8, expression of *RORβ* in layer 4 of the primary somatosensory area was altered in *TeNT* expressing mice, lacking the characteristic barrel pattern (Fig.7E.G). This is consistent with a recent study using *vGluT* mutants[53] and indicates the role of transmitter release in the formation of normal cytoarchitecture of the primary sensory cortex. In the PFC, however, induction of *Cyp26b1* in the medial and ventral PFC was not affected in TeNT-expressing mice (Fig.7F,H), revealing a unique cellular mechanism that underlies the induction of *Cyp26b1* expression in early postnatal PFC.

Discussion

In this study, we first demonstrated that *Cyp26b1*, which encodes a RA-degrading enzyme and is known as a critical regulator of retinoid signaling in development of many different organ systems[54,55], is expressed in developing PFC and that PV-expressing interneurons are a major cell population that normally responds to RA via the RAR/RXR receptors. Conditional deletion of *Cyp26b1* in frontal cortex resulted in an increased density of neurons that expressed *Pvalb* in medial PFC during postnatal development. Expression of *Cyp26b1* in the PFC depended on the interactions with the thalamus, but not on the transmitter release from thalamocortical axons. These results demonstrate a unique regulatory role of the thalamus in postnatal development of PV interneurons in the PFC (summarized in Fig.8D-G).

Roles of RA signaling in postnatal development of the medial PFC

In early embryonic brain, RA controls rostrocaudal patterning of the hindbrain and spinal cord by regulating the expression of *Hox* genes[19,20]. Cells in the subventricular zone of the lateral ganglionic eminence express the RA-synthesizing enzyme ALDH1A3, and *Aldh1a3* deficient mice showed a reduction of dopamine receptor D2 (*Drd2*) in nucleus accumbens[21] and *Gad1* in embryonic GABAergic neurons in the striatum and the neocortex[22], demonstrating a crucial role of RA in early differentiation of embryonic GABAergic neurons. However, much less is known about the roles of RA signaling in postnatal brain development. Systemic administration of RA into early postnatal mice caused behavioral hyperactivity at the adult stage with an increased number of calbindin-expressing neurons in the cingulate cortex [56]. Thus, it was

expected that RA has a major role in early postnatal brain development. However, the role of RA in PFC development and the underlying cellular and molecular mechanisms had remained unknown. Our current study revealed that in postnatal PFC, a subpopulation of PV interneurons are responsive to RA via RAR/RXR receptors, and the lack of the RA-degrading enzyme, CYP26B1, causes an increase in the number of *Pvalb*-expressing cells in medial PFC at P14 and P21. This phenotype should be independent of the known, earlier roles of RA in tangential migration of GABA neurons[57] because most MGE-derived interneurons have completed the tangential migration to the cortex by birth, and in our conditional knockout mice, *Cyp26b1* was deleted only postnatally. In addition, the increased number of *Pvalb*-positive neurons in deep layers of medial PFC was not accompanied by their decrease in upper layers. This suggests that the radial dispersion of PV neurons, which follows tangential migration, was also unaffected in *Cyp26b1* mutants. Interestingly, in adult *Cyp26b1* mutants, we no longer observed a significant increase in the number *Pvalb*-positive neurons in medial PFC (Fig.S4G-I), and we did not observe significant increase in the number of cells positive for cleaved Caspase-3 at P7 and P11 (data not shown). Thus, the combined evidence suggests that the main role of *Cyp26b1* in postnatal development of PV neurons in the medial PFC is to control their rate of maturation by suppressing RA signaling. Further studies are needed to investigate different aspects of maturation of PV neurons including electrophysiological properties, formation of perineural nets and changes in gene expression[14,58].

Universal and area-specific roles of the thalamus in neocortical development

Previous studies have indicated that thalamocortical afferents have instructive roles in establishing area- and layer-specific gene expression and in promoting morphological differentiation of excitatory neurons in primary visual and somatosensory cortex [33,53,59,60]. Although the underlying cellular and molecular mechanisms have just begun to be elucidated, at least some of the effects appear to be dependent on the release of neurotransmitters from the thalamocortical axon terminals[53]. In addition to excitatory neurons, both SST- and PV- interneurons also depend on thalamic afferents for their maturation, likely via glutamatergic synaptic transmission at early postnatal stages in somatosensory cortex[11–13]. In somatosensory, visual and motor areas, thalamic afferents also control radial positioning of MGE-derived interneurons before birth, in which the thalamus regulates the expression of the KCC2 cotransporter via the release of glutamate from the axon terminals[10]. Are these roles universal throughout the cortex or is there area-specific regulation of cortical development by the thalamus? The thalamus is composed of dozens of nuclei with distinct gene expression profiles[17,61], and each thalamic nucleus has a unique patterns of axonal projections to different cortical areas[18]. The neocortex is also regionally specified before the arrival of the thalamic axons, and exhibits a caudal-to-rostral developmental gradient [62]. Thus, it is expected that the nature of interactions with the thalamus varies between different cortical areas. In fact, expression of molecular markers that showed abnormal patterns in primary sensory cortex was not impaired in the medial PFC of *Gbx2* mutant mice (Fig.S5). Our current study has revealed a PFC-specific regulation of *Cyp26b1* expression by the thalamus at early postnatal stages in a manner independent of the VAMP2-mediated mechanism. Importantly, *Cyp26b1* was normally expressed in layer 6

in the frontal cortex and was conditionally deleted by *Syt6-Cre*, which is active in corticothalamic projection neurons (Allen Brain Atlas). Therefore, it is an intriguing possibility that the induction of *Cyp26b1* in the PFC depends on the arrival of corticothalamic axons in the thalamus, which is also disrupted in *Gbx2* mutant mice ([63] and this study). The current study also revealed an early role of the thalamus in regulating the radial positioning of MGE-derieved interneurons in neonatal PFC. This phenotype was highly reminiscent of what was found in sensory and motor areas[10], which strongly indicates that the early role of the thalamus in controlling the radial positions of cortical interneurons is shared between many neocortical areas (summarized in Fig.8A-C).

Functional implications of altered PV neuron development in *Cyp26b1* mutant mice

At the systems level, RA regulates cortical synchrony during sleep[64], memory and cognitive behaviors[65–67]. In addition, aberrant RA signaling is associated with multiple psychiatric disorders including schizophrenia, bipolar disorder and depression in humans[68–71]. Because many psychiatric disorders are predisposed by aberrant brain development, understanding how RA functions at early postnatal brain development is important for determining the long-term consequences of the perturbations of this signaling pathway. We found that in the absence of *Cyp26b1* in frontal cortex during a discrete period of postnatal development, the medial PFC had more *Pvalb*-expressing interneurons than in control mice. It is well established that PV neurons orchestrate activity in local circuits, which leads to oscillatory synchronous network activity in the

gamma-band[72,73]. Synchronous gamma-band activity in medial PFC is associated with the successful operation of working memory. In a mouse genetic model of schizophrenia that replicates the human the 22q11.2 microdeletion syndrome[74], both gamma synchrony and working memory performance were impaired[75] and development of PV interneurons were impaired[3,76–78]}. Furthermore, mutations in the *Disc1* gene, a significant risk factor not only for schizophrenia but other disorders including depression and bipolar disorder in humans, cause alterations of PV neurons and reduction of gamma oscillations in mice[79]. These findings link PV interneuron abnormalities to changes in prefrontal synchrony and working memory impairment in mouse models of neuropsychiatric disorders. Mutation of CYP26B1 in humans is a risk factor for schizophrenia that reaches genome wide significance[80,81]. Therefore, it will be interesting to test whether aberrant time course of PV neuron development in medial PFC causes altered synchrony and impairment of cognitive behaviors in *Cyp26b1* mutant mice.

Materials and methods

Mice. *RARE-LacZ* transgenic mice[28] were obtained from Jackson Laboratory (stock number: 008477) and were kept in the CD1 background. Frontal cortex-specific *Cyp26b1* mutant mice were generated using BAC (bacterial artificial chromosome) *Syt6-Cre* mice (*Syt6*$^{Cre/+}$) mice (GENSAT)[29,30]. Although the endogenous *Syt6* gene is expressed ubiquitously in layer 6 of the neocortex, the BAC Cre line caused recombination specifically in the frontal cortex. We crossed *Syt6*$^{Cre/+}$*; Cyp26b1*$^{flox/+}$ mice and *Cyp26b1*$^{flox/flox}$ mice to generate the conditional mutants. *Cyp26b1*$^{flox/flox}$ mice[31] were developed by Dr. Hiroshi Hamada's laboratory (RIKEN CDB, Kobe, Japan) and obtained from Dr. Maria Morasso (NIAMS, Bethesda, MD). *Rosa26*$^{stop\text{-}ZSGreen/+}$ (*Ai6*) mice[32] were obtained from Jackson Laboratory (stock number: 007906). Thalamus-specific *Gbx2* mutant mice were generated by crossing *Olig3*$^{Cre/+}$*; Gbx2*$^{null/+}$ mice and *Gbx2*$^{flox/flox}$ mice as described[33]. *Gbx2*$^{flox/flox}$ mice were obtained from Jackson Laboratory[34]. *Olig3*$^{Cre/+}$mice were described previously[35,36]. The *Gbx2*^{null} allele was generated by crossing *Gbx2*$^{flox/flox}$ mice with the *CMV-Cre* germ-line deleter mice (Jackson Laboratory, stock number: 003465). Mice that express tetanus toxin light chain in thalamic neurons were generated by crossing *Olig3*$^{Cre/+}$ mice and *Rosa26*$^{stop\text{-}TeNT/stop\text{-}TeNT}$ mice [37].

In situ hybridization. cDNAs for the following genes were used: *Cyp26b1*(Open Biosystems), *Aldh1a3* (Open Biosystems), *Syt6* (Open Biosystems), *Pvalb* (obtained from Dr. Rob Machold*)*, *Sst* (obtained from Dr. Rob Machold*), RORβ*, (obtained from Dr. Michael Becker-Andre) and *Lmo4* (Open Biosystems). Postnatal pups were perfused

with 4% paraformaldehyde/0.1M phosphate buffer and the heads were post-fixed until needed. Brains were then taken out of the skull, washed in 0.1M phosphate buffer for 20min and were sunk in 30% sucrose/0.1M phosphate buffer. Coronal sections were cut with a sliding microtome at 50μm-thickness (Leica) or with a cryostat at 20μm- (P2 or younger) or 40μm-thickness (P4 or older) and were mounted on glass slides (Super Frost Plus, Fisher). In situ hybridization was carried out as described [38].

Immunohistochemistry. Brains were taken out immediately after perfusion and were postfixed for 1 hour (P0), 2 hours (P4-P14) or 4 hours (P21). After the post-fixation, the brains were washed in 0.1M phosphate buffer for 20min and were sunk in 30% sucrose/ 0.1M phosphate buffer. Sections were cut in the same way as those used for in situ hybridization. The following primary antibodies were used: β-galactosidase (Cappel, 55976, goat, 1:100), SOX6 (Abcam, rabbit, 1:100), SP8 (Santa Cruz, sc-104661, goat, 1:100), CTIP2 (Abcam ab18465, rat, 1:200), TBR1 (Abcam, ab31940, rabbit, 1:200; Millipore, AB2261, chicken, 1:200), PV (SWANT, rabbit, 1:500), SST (Millipore, MAB354, rat, 1:100), LHX6 (Santa Cruz, sc-271433, mouse, 1:50), VAMP2 (Synaptic Systems, 104 202, rabbit, 1:200), NetrinG1 (R&D Systems, goat, 1:100). Secondary antibodies conjugated with Cy2, Cy3 or Cy5 were obtained from Jackson ImmunoResearch.

Imaging/Binning. For cell counting, images of sections that underwent in situ hybridization or immunostaining were taken using a fluorescence microscope (Nikon E800) with a 2x (in situ hybridization) or a 4x (immunostaining) objective using a digital

CCD camera (Retiga EXi, QImaging) and the OpenLab software. The range of coronal sections to be included in the analysis of medial PFC was defined rostrally by the presence of the lateral ventricle and caudally by the presence of the anterior forceps of the corpus callosum. Once the sections were selected, their images were scrambled and each file was given a randomized number so that the person who performed the subsequent analysis was made blind to the genotypes. Cell counting was performed in the putative prelimbic (PL) and infralimbic (IL) areas of the medial PFC (Allen Brain Atlas; [39,40]). Images were stacked using Adobe Photoshop and subsequently binned to distinguish the parts of the medial PFC as shown in Fig.4; each bin is 500μm-high at the medial surface. For sections with in situ hybridization, the most superficial layer (layer 1) was defined as the cell-sparse layer on DAPI staining. The remaining cortical wall was divided into three bins with equal widths, resulting in 4 layers of bins. Layer 1 and the layer underneath it were named superficial layers and the remaining two layers were named the deep layers. For immunostaining, we used anti-TBR1 antibody for all slides in Cy5 channel and used it as a reference marker of layer 6. Then, the areas excluding layers 1 and 6 were equally divided into three parts, resulting in four layers of bins (shown in Fig.6).

Cell Counting. In imageJ, the Image-based Tool for Counting Nuclei (ITCN) plugin, from the Center for Bio-Image Informatics, UC Santa Barbara, was used to count cells and measure the area of each bin.

Statistical analysis. Paired ratio t-test was used for comparing cell counts between *Gbx2* cko mice and wild-type littermates as well as *Cyp26b1* cko and wild-type littermates. Comparison was always made between two brains processed and analyzed in the same experiment. The analysis was done blind to the genotype. GraphPad Prism (versions 6 and 7) was used for all statistical analyses and graph production.

Axon tracing. Small crystals of 1,1′-dioctadecyl-3,3,3′3′-tetramethylindocarbocyanine perchlorate (DiI) were placed on the medial surface of frontal cortex of PFA-fixed P14 *Gbx2* conditional mutant brains and their control littermates. After incubation of the brains in PFA at 37c for 2 weeks, we cut sections at 150μm with a vibrating microtome (Vibratome), counter-stained the sections and mounted them on glass slides for imaging.

Acknowledgments

We also thank Steven McLoon, Goichi Miyoshi and Tim Monko for helpful comments and discussions, and Earl Parker Scott, Thomas Bao, Shaylene McCue, Morgan McCullough and Carmen Tso for technical assistance. Zachery Werkhoven and Melody Lee contributed to the initial phase of the project. We thank Martyn Goulding for providing *Rosa26*$^{\text{stop-TeNT/+}}$ mice, Hiroshi Hamada (RIKEN Center for Developmental Biology) and Maria Morasso (NIH) for *Cyp26b1*$^{\text{flox/+}}$ mice and Eric Turner (University of Washington) for *Syt6*$^{\text{Cre/+}}$ mice, Rob MacHold for *Pvalb* and *Sst* cDNAs. This work was supported by grants to Y.N. from NIH (R21MH105759), Brain and Behavior Research Foundation, Winston and Maxim Wallin Neuroscience Discovery Fund and Academic Health Center of the University of Minnesota.

References

1. Schubert, D., Martens, G. J. & Kolk, S. M. Molecular underpinnings of prefrontal cortex development in rodents provide insights into the etiology of neurodevelopmental disorders. *Mol Psychiatry* **20**, 795-809 (2015).
2. Caballero, A. & Tseng, K. Y. GABAergic Function as a Limiting Factor for Prefrontal Maturation during Adolescence. *Trends Neurosci* **39**, 441-448 (2016).
3. Meechan, D. W., Tucker, E. S., Maynard, T. M. & LaMantia, A. S. Cxcr4 regulation of interneuron migration is disrupted in 22q11.2 deletion syndrome. *Proc Natl Acad Sci U S A* **109**, 18601-18606 (2012).
4. Hashemi, E., Ariza, J., Rogers, H., Noctor, S. C. & Martínez-Cerdeño, V. The Number of Parvalbumin-Expressing Interneurons Is Decreased in the Medial Prefrontal Cortex in Autism. *Cereb Cortex* (2016).
5. Powell, S. B., Sejnowski, T. J. & Behrens, M. M. Behavioral and neurochemical consequences of cortical oxidative stress on parvalbumin-interneuron maturation in rodent models of schizophrenia. *Neuropharmacology* **62**, 1322-1331 (2012).
6. Nakazawa, K. et al. GABAergic interneuron origin of schizophrenia pathophysiology. *Neuropharmacology* **62**, 1574-1583 (2012).
7. Gonzalez-Burgos, G., Cho, R. Y. & Lewis, D. A. Alterations in cortical network oscillations and parvalbumin neurons in schizophrenia. *Biol Psychiatry* **77**, 1031-1040 (2015).
8. Chu, J. & Anderson, S. A. Development of cortical interneurons. *Neuropsychopharmacology* **40**, 16-23 (2015).
9. Wamsley, B. & Fishell, G. Genetic and activity-dependent mechanisms underlying interneuron diversity. *Nat Rev Neurosci* **18**, 299-309 (2017).
10. Zechel, S., Nakagawa, Y. & Ibáñez, C. F. Thalamo-cortical axons regulate the radial dispersion of neocortical GABAergic interneurons. *Elife* **5**, (2016).
11. Sugiyama, S. et al. Experience-dependent transfer of Otx2 homeoprotein into the visual cortex activates postnatal plasticity. *Cell* **134**, 508-520 (2008).
12. Marques-Smith, A. et al. A Transient Translaminar GABAergic Interneuron Circuit Connects Thalamocortical Recipient Layers in Neonatal Somatosensory Cortex. *Neuron* **89**, 536-549 (2016).
13. Tuncdemir, S. N. et al. Early Somatostatin Interneuron Connectivity Mediates the Maturation of Deep Layer Cortical Circuits. *Neuron* **89**, 521-535 (2016).
14. Ueno, H., Suemitsu, S., Okamoto, M., Matsumoto, Y. & Ishihara, T. Parvalbumin neurons and perineuronal nets in the mouse prefrontal cortex. *Neuroscience* **343**, 115-127 (2017).
15. Gonchar, Y., Wang, Q. & Burkhalter, A. Multiple distinct subtypes of GABAergic neurons in mouse visual cortex identified by triple immunostaining. *Front Neuroanat* **1**, 3 (2007).
16. Nowicka, D., Soulsby, S., Skangiel-Kramska, J. & Glazewski, S. Parvalbumin-containing neurons, perineuronal nets and experience-dependent plasticity in murine barrel cortex. *Eur J Neurosci* **30**, 2053-2063 (2009).
17. Nagalski, A. et al. Molecular anatomy of the thalamic complex and the underlying transcription factors. *Brain Struct Funct* **221**, 2493-2510 (2016).

18. Clasca, F., Rubio-Garrido, P. & Jabaudon, D. Unveiling the diversity of thalamocortical neuron subtypes. *Eur J Neurosci* **35**, 1524-1532 (2012).
19. Maden, M., Gale, E., Kostetskii, I. & Zile, M. Vitamin A-deficient quail embryos have half a hindbrain and other neural defects. *Curr Biol* **6**, 417-426 (1996).
20. Dupé, V. & Lumsden, A. Hindbrain patterning involves graded responses to retinoic acid signalling. *Development* **128**, 2199-2208 (2001).
21. Molotkova, N., Molotkov, A. & Duester, G. Role of retinoic acid during forebrain development begins late when Raldh3 generates retinoic acid in the ventral subventricular zone. *Dev Biol* **303**, 601-610 (2007).
22. Chatzi, C., Brade, T. & Duester, G. Retinoic acid functions as a key GABAergic differentiation signal in the basal ganglia. *PLoS Biol* **9**, e1000609 (2011).
23. Chen, N. & Napoli, J. L. All-trans-retinoic acid stimulates translation and induces spine formation in hippocampal neurons through a membrane-associated RARalpha. *FASEB J* **22**, 236-245 (2008).
24. Gonzalez-Quevedo, R., Lee, Y., Poss, K. D. & Wilkinson, D. G. Neuronal regulation of the spatial patterning of neurogenesis. *Dev Cell* **18**, 136-147 (2010).
25. Hernandez, R. E., Putzke, A. P., Myers, J. P., Margaretha, L. & Moens, C. B. Cyp26 enzymes generate the retinoic acid response pattern necessary for hindbrain development. *Development* **134**, 177-187 (2007).
26. Yashiro, K. et al. Regulation of retinoic acid distribution is required for proximodistal patterning and outgrowth of the developing mouse limb. *Dev Cell* **6**, 411-422 (2004).
27. Wagner, E., Luo, T., Sakai, Y., Parada, L. F. & Dräger, U. C. Retinoic acid delineates the topography of neuronal plasticity in postnatal cerebral cortex. *Eur J Neurosci* **24**, 329-340 (2006).
28. Rossant, J., Zirngibl, R., Cado, D., Shago, M. & Giguere, V. Expression of a retinoic acid response element-hsplacZ transgene defines specific domains of transcriptional activity during mouse embryogenesis. *Genes Dev* **5**, 1333-1344 (1991).
29. Gong, S. et al. A gene expression atlas of the central nervous system based on bacterial artificial chromosomes. *Nature* **425**, 917-925 (2003).
30. Hsu, Y. W. et al. Role of the dorsal medial habenula in the regulation of voluntary activity, motor function, hedonic state, and primary reinforcement. *J Neurosci* **34**, 11366-11384 (2014).
31. Okano, J. et al. Increased retinoic acid levels through ablation of Cyp26b1 determine the processes of embryonic skin barrier formation and peridermal development. *J Cell Sci* **125**, 1827-1836 (2012).
32. Madisen, L. et al. A robust and high-throughput Cre reporting and characterization system for the whole mouse brain. *Nat Neurosci* **13**, 133-140 (2010).
33. Vue, T. Y. et al. Thalamic control of neocortical area formation in mice. *J Neurosci* **33**, 8442-8453 (2013).
34. Li, J. Y., Lao, Z. & Joyner, A. L. Changing requirements for Gbx2 in development of the cerebellum and maintenance of the mid/hindbrain organizer. *Neuron* **36**, 31-43 (2002).
35. Vue, T. Y. et al. Sonic hedgehog signaling controls thalamic progenitor identity and nuclei specification in mice. *J Neurosci* **29**, 4484-4497 (2009).

36. Bluske, K. K. et al. beta-Catenin signaling specifies progenitor cell identity in parallel with Shh signaling in the developing mammalian thalamus. *Development* **139**, 2692-2702 (2012).
37. Zhang, Y. et al. V3 spinal neurons establish a robust and balanced locomotor rhythm during walking. *Neuron* **60**, 84-96 (2008).
38. Vue, T. Y. et al. Characterization of progenitor domains in the developing mouse thalamus. *J Comp Neurol* **505**, 73-91 (2007).
39. Van De Werd, H. J., Rajkowska, G., Evers, P. & Uylings, H. B. Cytoarchitectonic and chemoarchitectonic characterization of the prefrontal cortical areas in the mouse. *Brain Struct Funct* **214**, 339-353 (2010).
40. Paxinos, G., Halliday, G. M., Watson, C., Koutcherov, Y. & Wang, H. *Atlas of the Developing Mouse Brain at E17.5, P0 and P6* (Academic Press, 2006).
41. Ng, L. et al. An anatomic gene expression atlas of the adult mouse brain. *Nat Neurosci* **12**, 356-362 (2009).
42. Wagner, E., Luo, T. & Dräger, U. C. Retinoic acid synthesis in the postnatal mouse brain marks distinct developmental stages and functional systems. *Cereb Cortex* **12**, 1244-1253 (2002).
43. Batista-Brito, R. et al. The cell-intrinsic requirement of Sox6 for cortical interneuron development. *Neuron* **63**, 466-481 (2009).
44. Ma, T. et al. A subpopulation of dorsal lateral/caudal ganglionic eminence-derived neocortical interneurons expresses the transcription factor Sp8. *Cereb Cortex* **22**, 2120-2130 (2012).
45. Arlotta, P. et al. Neuronal subtype-specific genes that control corticospinal motor neuron development in vivo. *Neuron* **45**, 207-221 (2005).
46. Chen, B., Schaevitz, L. R. & McConnell, S. K. Fezl regulates the differentiation and axon targeting of layer 5 subcortical projection neurons in cerebral cortex. *Proc Natl Acad Sci U S A* **102**, 17184-17189 (2005).
47. Nikouei, K., Muñoz-Manchado, A. B. & Hjerling-Leffler, J. BCL11B/CTIP2 is highly expressed in GABAergic interneurons of the mouse somatosensory cortex. *J Chem Neuroanat* **71**, 1-5 (2016).
48. Fogarty, M. et al. Spatial genetic patterning of the embryonic neuroepithelium generates GABAergic interneuron diversity in the adult cortex. *J Neurosci* **27**, 10935-10946 (2007).
49. Miyoshi, G., Butt, S. J., Takebayashi, H. & Fishell, G. Physiologically distinct temporal cohorts of cortical interneurons arise from telencephalic Olig2-expressing precursors. *J Neurosci* **27**, 7786-7798 (2007).
50. Inamura, N. et al. Intrinsic and extrinsic mechanisms control the termination of cortical interneuron migration. *J Neurosci* **32**, 6032-6042 (2012).
51. Miyoshi, G. & Fishell, G. GABAergic interneuron lineages selectively sort into specific cortical layers during early postnatal development. *Cereb Cortex* **21**, 845-852 (2011).
52. Nakashiba, T., Nishimura, S., Ikeda, T. & Itohara, S. Complementary expression and neurite outgrowth activity of netrin-G subfamily members. *Mech Dev* **111**, 47-60 (2002).
53. Li, H. et al. Laminar and columnar development of barrel cortex relies on thalamocortical neurotransmission. *Neuron* **79**, 970-986 (2013).

54. Rhinn, M. & Dolle, P. Retinoic acid signalling during development. *Development* **139**, 843-858 (2012).
55. Duester, G. Retinoic acid synthesis and signaling during early organogenesis. *Cell* **134**, 921-931 (2008).
56. Luo, T., Wagner, E., Crandall, J. E. & Drager, U. C. A retinoic-acid critical period in the early postnatal mouse brain. *Biol Psychiatry* **56**, 971-980 (2004).
57. Crandall, J. E. et al. Retinoic acid influences neuronal migration from the ganglionic eminence to the cerebral cortex. *J Neurochem* **119**, 723-735 (2011).
58. Okaty, B. W., Miller, M. N., Sugino, K., Hempel, C. M. & Nelson, S. B. Transcriptional and electrophysiological maturation of neocortical fast-spiking GABAergic interneurons. *J Neurosci* **29**, 7040-7052 (2009).
59. Moreno-Juan, V. et al. Prenatal thalamic waves regulate cortical area size prior to sensory processing. *Nat Commun* **8**, 14172 (2017).
60. Chou, S. J. et al. Geniculocortical input drives genetic distinctions between primary and higher-order visual areas. *Science* **340**, 1239-1242 (2013).
61. Jones, E. G. *The Thalamus* (Cambridge University Press, Cambridge ; New York, 2007).
62. Bayer, S. & Altman, J. in *Neocortical Development* 30-45 (Raven Press, New York, 1991).
63. Hevner, R. F., Miyashita-Lin, E. & Rubenstein, J. L. Cortical and thalamic axon pathfinding defects in Tbr1, Gbx2, and Pax6 mutant mice: evidence that cortical and thalamic axons interact and guide each other. *J Comp Neurol* **447**, 8-17 (2002).
64. Maret, S. et al. Retinoic acid signaling affects cortical synchrony during sleep. *Science* **310**, 111-113 (2005).
65. Chiang, M. Y. et al. An essential role for retinoid receptors RARbeta and RXRgamma in long-term potentiation and depression. *Neuron* **21**, 1353-1361 (1998).
66. Aoto, J., Nam, C. I., Poon, M. M., Ting, P. & Chen, L. Synaptic signaling by all-trans retinoic acid in homeostatic synaptic plasticity. *Neuron* **60**, 308-320 (2008).
67. Nomoto, M. et al. Dysfunction of the RAR/RXR signaling pathway in the forebrain impairs hippocampal memory and synaptic plasticity. *Mol Brain* **5**, 8 (2012).
68. Goodman, A. B. Three independent lines of evidence suggest retinoids as causal to schizophrenia. *Proc Natl Acad Sci U S A* **95**, 7240-7244 (1998).
69. Qi, X. R. et al. Abnormal Retinoid and TrkB Signaling in the Prefrontal Cortex in Mood Disorders. *Cereb Cortex* (2013).
70. Haybaeck, J. et al. Increased expression of retinoic acid-induced gene 1 in the dorsolateral prefrontal cortex in schizophrenia, bipolar disorder, and major depression. *Neuropsychiatr Dis Treat* **11**, 279-289 (2015).
71. Bremner, J. D., Shearer, K. D. & McCaffery, P. J. Retinoic acid and affective disorders: the evidence for an association. *J Clin Psychiatry* **73**, 37-50 (2012).
72. Cardin, J. A. et al. Driving fast-spiking cells induces gamma rhythm and controls sensory responses. *Nature* **459**, 663-667 (2009).
73. Sohal, V. S., Zhang, F., Yizhar, O. & Deisseroth, K. Parvalbumin neurons and gamma rhythms enhance cortical circuit performance. *Nature* **459**, 698-702 (2009).

74. Karayiorgou, M. et al. Schizophrenia susceptibility associated with interstitial deletions of chromosome 22q11. *Proc Natl Acad Sci U S A* **92**, 7612-7616 (1995).
75. Sigurdsson, T., Stark, K. L., Karayiorgou, M., Gogos, J. A. & Gordon, J. A. Impaired hippocampal-prefrontal synchrony in a genetic mouse model of schizophrenia. *Nature* **464**, 763-767 (2010).
76. Fénelon, K. et al. The pattern of cortical dysfunction in a mouse model of a schizophrenia-related microdeletion. *J Neurosci* **33**, 14825-14839 (2013).
77. Meechan, D. W. et al. Cognitive ability is associated with altered medial frontal cortical circuits in the LgDel mouse model of 22q11.2DS. *Cereb Cortex* **25**, 1143-1151 (2015).
78. Toritsuka, M. et al. Deficits in microRNA-mediated Cxcr4/Cxcl12 signaling in neurodevelopmental deficits in a 22q11 deletion syndrome mouse model. *Proc Natl Acad Sci U S A* **110**, 17552-17557 (2013).
79. Sauer, J. F., Strüber, M. & Bartos, M. Impaired fast-spiking interneuron function in a genetic mouse model of depression. *Elife* **4**, (2015).
80. Mistry, M., Gillis, J. & Pavlidis, P. Genome-wide expression profiling of schizophrenia using a large combined cohort. *Mol Psychiatry* **18**, 215-225 (2013).
81. Schizophrenia, W. G. O. T. P. G. C. Biological insights from 108 schizophrenia-associated genetic loci. *Nature* **511**, 421-427 (2014).

FIGURE LEGENDS

Fig.1 Transient expression of *Cyp26b1* in the PFC.

In situ hybridization of frontal sections through PFC at various postanatal stages is shown. **A,B.** *Cyp26b1* expression in frontal cortex. At P2, *Cyp26b1* starts to be detected in medial PFC (arrowhead in A). Expression in lateral cortex, especially agranular insula in more superficial layer (double arrowheads) is strong, which continues into later stages (arrowhead in B,E,F). At P8, expression in medial (arrowhead) and ventral (arrow) PFC is strong (B). **C,D.** In sections adjacent to B, *Aldh1a3* is expressed immediately below layer 1 (C). *Synaptotagmin-6* (*Syt6*), a layer 6 marker, is expressed in the same location as *Cyp26b1* in medial PFC (arrowhead in D) at P8. **E,F.** At P21, expression of *Cyp26b1* is reduced in medial PFC (arrowhead in E) and is almost undetectabe by P35 (arrowhead in F). **G.** Schematic summary of the spatial and temporal expression patterns of *Cyp26b1* and *Aldh1a3* in medial PFC of early postnatal mouse brains. Expression of *Aldh1a3* is also based on Wagner et al. (2006).

Fig.2 RA singlaing in early postnatal PFC.

In all sections, medial suface of the brain is to the left. Immunostaining for β-gal on frontal sections of P0 (A), P8 (B-E) and P14 (F-K) brains of *RARE-LacZ* transgenic mice. **A.** At P0, β-gal expression is only found in the radial glial fibers. **B-E.** At P7, β-gal expression starts to be detected in SOX6-expressing cells in medial PFC. Most β-gal-positive cells are also SOX6-positive (yellow arrows showing double-labeled cells) except some in the superficial layers (white arrowhead showing single-labeled cells). β-gal does not overlap with SP8, CTIP2 or TBR1. **F-K.** At P14, the number of β-gal-

positive cells dramatically increased compared with P7, and almost all β-gal-positive cells are SOX6-positive (F and G show signle labeling of β-gal and SOX6, respectively, of the boxed area in H). Yellow arrows show double-labeled cells. (I-K) β-gal doses not overlap with SP8, CTIP2 or TBR1. Scale bar, 100ㄱm. **L.** Average number of β-gal-positive cells per section by layers (mean ± SEM). L1, layer 1 as marked by sparse labeling in DAPI staiing. L6, layer 6 as marked by TBR1 staining. The two middle columns represent equal-width bins between layer 1 and layer 6, and roughtly corresond to layers 2/3 and layer 4/5, respectively. Because most β-gal-positive cells are immediately above layer 6 and layer 4 is thin in medial PFC (Fig.S2A), the highest peak in the third column likely represents layer 5. **M**. The ratio of SOX6; β-gal-double-positive cells among β-gal-positive cells are shown by layers (mean ± SEM).

Fig.3 Overlap of *RARE-LacZ* transgene expression and Parvalbumin in early postnatal PFC.

A-C. In situ hybridization of *Pvalb* mRNA on frontal sections of control mice at P8 (A), P14 (B) and P21 (C). **D-G.** Immunostaining for β-gal on frontal sections of P8 (D), P14 (E,F) and P21 (G) brains of *RARE-LacZ* transgenic mice. F' and G' are higher magnifications of the inset in F and G, respectively. Overlap between β-gal and PV is shown by yellow arrows. Scale bar, 500ㄱm (A,B,C,F,G) or 200ㄱm (D,E,F',G'). **H.** The ratio of PV; β-gal-double-positive cells among β-gal-positive cells are shown by layers (mean ± SEM). **I.** The ratio of PV; β-gal-double-positive cells among PV-positive cells are shown by layers (mean ± SEM). **J.** Schematic summary of the interneuron

populations in medial PFC. Based on the results in this study, a subpopulation of PV interneurons respond to RA via RAR/RXR receptor complex.

Fig.4 Increased *Pvalb*-expressing interneurons in medial PFC of *Cyp26b1* knockout mice.

A-B,D-E. In situ hybridization of frontal sections of P14 (**A,B**) and P21 (**C,D**) *Cyp26b1* conditional knockout mice (**B,E**) and littermate controls (**A,D**). Expression of *Parvalbumin* (*Pvalb*) is shown. See Methods for how to make bins within medial PFC. Numbers of *Pvalb*-positive cells in the two superficial bins and two deep bins were added together and compared separately between *Cyp26b1* mutants and littermate controls. **C** and **F** show the result of statistical analysis. Each line connecting red and blue dots represents a pair of brains analyzed in the same experiment (n=5). *; $p<0.05$., n.s.; not significant. Scale bar, 1mm. L1: layer 1

Fig.5 Transient expression of *Cyp26b1* in the PFC does not occur in the absence of thalamus-cortex interactions in *Gbx2* mutant mice.

A-J. in situ hybridization of frontal sections through PFC at various postanatal stages with a *Cyp26b1* probe. G amd N show in situ hybridization of P4 frontal sections for *Synaptotagmin 6* (*Syt6*). **A-E.** In control mice, *Cyp26b1* expression starts in medial (arrowhead) and ventral (single arrow) PFC at P2 (A) and continues until P14 (C). At P21, expression in medial PFC is reduced (D) and is no longer detectable at P35 (E). In addition to medial and ventral PFC, *Cyp26b1* is also expressed in lateral frontal cortex including the motor area (double arrows) and agranular insula (double arrowheads).

F-J. In *Gbx2* mutant mice, expression of *Cyp26b1* is not induced in medial PFC at P2 as well as at later stages. Expression in more superficial layer of lateral cortex (double arrows and double arrowheads) is not affected in *Gbx2* mutant mice. **K,N.** Expression of the layer 6 marker *Syt6* is not affected in *Gbx2* mutant mice. **L,O.** Expression of *Aldh1a3* in layer 2 of medial PFC and anterior cingulate cortex (arrow) is not affected in *Gbx2* mutant mice. scale bar, 1mm. **M,P.** Summary schematic.

Fig.6 Abnormal numbers of interneurons in the medial PFC of *Gbx2* mutant mice.

A-C. Comparison of *Pvalb*-positive and *Sst*-positive cells in *Gbx2* mutants (blue dots) and wild-type littermates (red dots) in medial PFC at P21. Each line connecting red and blue dots represents a pair of brains analyzed in the same experiment (n=5). **A** and **B** show laminar distribution of *Pvalb*-expresing and Sst-expressing neurons, respectively. Layer 1 was defined as the cell-sparse layer detected by DAPI staining. The remaining cortical wall was equally divided into three layers. The deepest layer (shown as “L5/6”) contains the entire layer 6 and the deep part of layer 5. **C** shows the total number of *Pvalb*- and *Sst*-expressing neurons in all layers. **D-E.** Representative images of immunostaining for LHX6 in medial PFC of wild-type **(D)** and *Gbx2* cko **(E)** mice at P0. Binning is shown in yellow. Layer 1 (L1) was defined as the cell-sparse layer detected by DAPI staining. Layer 6 (L6) was defined as the layer with TBR1 staining on the same sections (not shown). The intervening region was equally divided into three layers. Sub-layer 6 was defined as the layer below layer 6. Scale bar, 200ㄱm **F-G.** Comparison of LHX6-positive cells in *Gbx2* mutants (blue dots) and wild-type littermates (red dots) in medial PFC at P0. Each line connecting red and blue dots represents a pair of brains

analyzed in the same experiment (n=5). **F** shows laminar distribution pattern. **G** shows the total number of *Pvalb*- and *Sst*-expressing neurons in all layers. “Sub-L6” was defined as the region below the expression domain of TBR1, which was stained in all immunostaining slides for a reference *: $p<0.05$

Fig.7 Normal induction of *Cyp26b1* in PFC in mice expressing tetanus toxin light chain in thalamocortical axons.

A-D. Immunostaining for VAMP2 on frontal sections of E16.5 control (A,B) and mutant mice with ectopic expression of tetanus toxin light chain (TeNT) in thalamic neurons (C,D). TeNT expression leads to deletion of VAMP2 specifically in thalamocortical axons at E16.5. Thalamocortical axons are shown by NetrinG1 staining (B,D, green). In control brains, both thalamocortical (shown in asterisk in A-D) and corticofugal (shown in bracket in A-D) express VAMP2, whereas in TeNT-expressing mice, VAMP2 staining is specifically diminished in thalamocortical axons. Scale bar, 500**μ**m

E.G. Deletion of VAMP2 in thalamocortical axons results in the lack of the characterisitc pattern of *RORβ* expression in the barrel field of primar somatosesoy cortex at P8 (G), similar to the defect found in *Gbx2* mutant mice (Vue et al., 2013).

F,H. Expression of *Cyp26b1* in medial (arrowhead) and ventral PFC is intact in TeNT-expressing mice at P8. scale bar, 1mm

Fig.8 Schmatic diagrams of the current finding.

A-C. Embryonic roles of thalamocortical axons as observed in neonatal mice. (A) Thalamocortical axons reach the medial PFC (mPFC) by E16.5 and control migration of

medial ganglionic eminence (MGE0-derived interneurons likely by employing glutamate release from the axon terminals. (B) In normal neonatal mice, MGE-derived interneurons have largely completed tangential migration to the mPFC and have taken proper laminar positioning by radial dispersion (arrows). (C) In thalamus-specific *Gbx2* mutant mice, radial positioning of MGE-derived interneurons are aberrant, resulting in their accumulation in layer 6. **D-G.** Postnatal roles of thalamus-PFC interactions and retinoic acid (RA)-degrading enzyme CYP26B1 in the development of PV interneurons in the mPFC. (D) Early postnatal mPFC is positioned between the source of RA synthesis (layer 2, by ALDH1A3) and the RA-degrading "sink" (layer 6, by CYP26B1). Expression of both enzymes are induced early postnatally, but only *Cyp26b1* is dependent on the connections with the thalamus. The main cell population that responds to RA in postnatal mPFC are parvalbumin (PV) interneurons, and their development is controlled by CYP26B1. (E) In normal postnatal mice, PV neurons mature and start to express *Pvalb* mRNA and PV protein mainly in deep layers of mPFC between P7 and P14. (F) In thalamus-specific *Gbx2* mutant mice, *Cyp26b1* is not induced in mPFC. The number of both *Pvalb* and *Somatostatin* (*Sst*)-expressing neurons is reduced in the middle layers due to the earlier defects in radial dispersion (described in C). (G) In frontal cortex-specific *Cyp26b1* mutant mice, lack of the RA sink in mPFC leads to an increased number of neurons that express *Pvalb* mRNA or PV protein in deep layers.

LEGENDS TO SUPPLEMENTAL FIGURES

Fig.S1 Normal expression pattern of *Cyp26b1* in the mouse forebrain.

In situ hybridization on coronal sections is shown. **A.** Expression is not detected in the prefrontal cortex at E17.5 (arrowhead). **B.** At P0, middle layers of lateral cortex starts to express Cyp26b1. The prosective piriform cortex shows a strong exrpession (arrow). Expression in medial cortex is barely detectable (arrowhead). **C-E.** Expression in non-neocortical forebrain regions at E16.5 (C) and P4 (D,E). Already at E16.5, *Cyp26b1* is detected in hippocampus (C, arrowhead), piriform cortex (C,"Pir"), globus pallidus and amygdala (C, arows). This pattern continues into P4 (D,E,) and adulthood (not shown). E is at a more caudal level than D. Expression in the hippocampus is strongest in CA3 and hilus, whereas multiple nuclei in amydala show strong expressoin of *Cyp26b1* (E). scale bar=1mm.

Fig.S2 Generation of *Cyp26b1* cko mice.

A-F. In situ hybridization of frontal sections of P8 *Cyp26b1* conditional knockout (**B,D,F**) and control littermate (**A,C,E**) brains. *Cyp26b1* was knocked out using the *Synaptotagmin-Cre* (*Syt6-Cre*) transgene. **A,B.** *Syt6* is expressed both in layer 6 of both control (**A**) and *Cyp26b1* knockout (**B**) brain (arrow). **C,D.** Expression of *Cyp26b1* in layer 6 of frontal cortex (arrow) is detected in control (**C**), but not in *Cyp26b1* knockout brain (**D**). Expression of *Cyp26b1* in agranular insula (arrowhead) is unchangd in *Cyp26b1* knockouts. **E,F.** Expression of *Cyp26b1* in CA3 region of the hippocampus (arrowhead) is unchangd in *Cyp26b1* knockouts. Scale bar, 1mm.

Fig.S3 No significant changes in the number of *Sst*-, *Vip*- and *Lhx6*-expressing interneurons in medial PFC of *Cyp26b1* knockout mice at P14 and P2.

A-D. In situ hybridization of frontal sections of P14 *Cyp26b1* conditional knockout mice (**C,D**) and littermate controls (**A,B**). Expression of *Somatostatin (Sst)* (**A,C**)*, Vip* (**B,D**) is shown. Binning and cell counts were done in the same was as shown in Fig.6 for *Pvalb*-expressing cells. **E-I.** Result of statistical analysis. Each line connecting red and blue dots represents a pair of brains analyzed in the same experiment (n=5). n.s.; not significant. Scale bar, 1mm. **G-I.** No significant changes in the number of *Pvalb*-, *Sst*- and *Vip*-expressing interneurons in medial PFC of adult (P56-P67) *Cyp26b1* knockout mice. Each line connecting red and blue dots represents a pair of brains analyzed in the same experiment (n=4).

Fig.S4: Thalamus-PFC disconnection in *Gbx2* mutant mice.

A, B. NetrinG1 immunostaining at E16.5. In control mice, NetrinG1-labeled thalamocortical axons are visible in coronal sections of frontal cortex. Arrowhead in A shows the medial PFC, where robust labeling is detected. In contrast, NetrinG1-labeling is undetectable in the frontal cortex of *Gbx2* mutant mice, including the medial PFC (arrowhead in B). scale bar, 200μm.

C-F. DiI labeling at P14. DiI placement in medial PFC retrogradely labels thalamic nuclei (show more details) in the control brains (**C,D**). In *Gbx2* mutants, the label is severely reduced (**E,F**), indicating the deficiency of both thalamocortical and corticothalamic projections.

Fig.S5 Expression of *RORβ* and *Lmo4* are qualitatively normal in the PFC of *Gbx2* mutant mice at postnatal day 8 (P8).

A,B. Expression of *RORβ* in layer 4 is comparable between conrol and *Gbx2* mutant (cko) mice (arrows). **C,D.** Laminar expression patterns of *Lmo4* also appear unchanged in *Gbx2* mutants. scale bar=1mm.

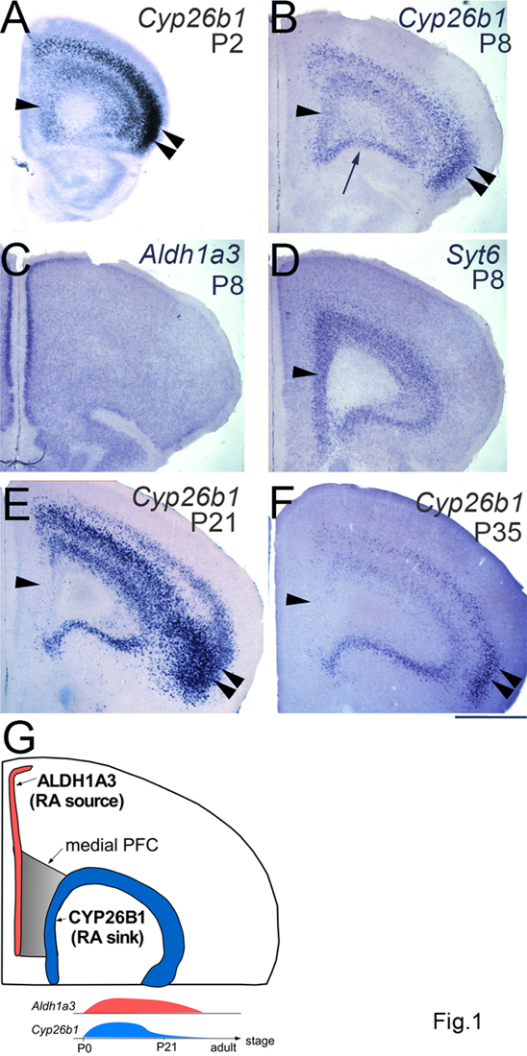
A
Cyp26b1
P2
B
Cyp26b1
P8
C
Aldh1a3
P8
D
Syt6
P8
E
Cyp26b1
P21
F
Cyp26b1
P35
G
ALDH1A3
(RA source)
medial PFC
CYP26B1
(RA sink)
Aldh1a3
Cyp26b1
stage
P0
P21
adult

Fig.1

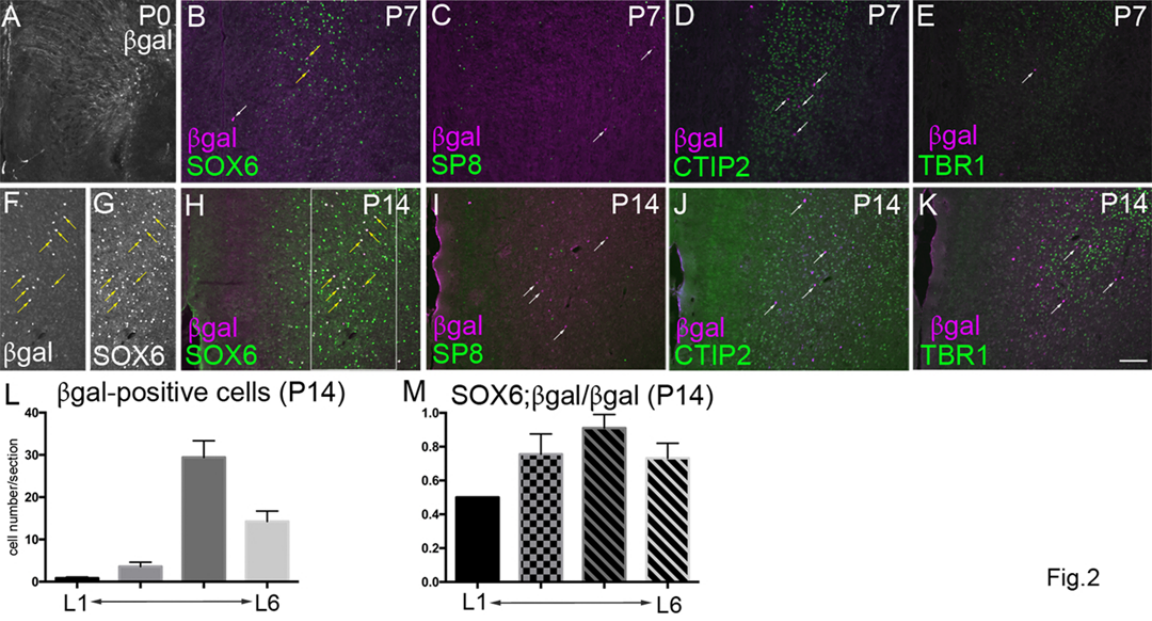
A
P0
βgal
B
P7
βgal
SOX6
C
P7
βgal
SP8
D
P7
βgal
CTIP2
E
P7
βgal
TBR1
F
βgal
G
SOX6
H
P14
βgal
SOX6
I
P14
βgal
SP8
J
P14
βgal
CTIP2
K
P14
βgal
TBR1
L
βgal-positive cells (P14)
cell number/section
40
30
20
10
0
L1
L6
M
SOX6;βgal/βgal (P14)
1.0
0.8
0.6
0.4
0.2
0.0
L1
L6

Fig.2

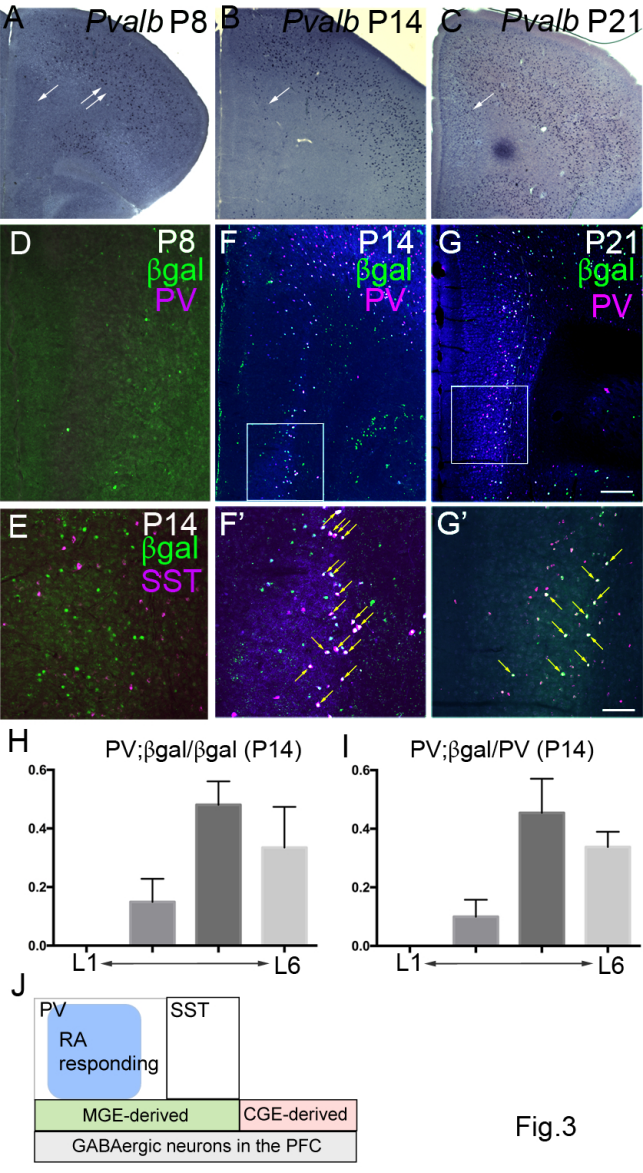
A
Pvalb P8
B
Pvalb P14
C
Pvalb P21
D
P8
βgal
PV
F
P14
βgal
PV
G
P21
βgal
PV
E
P14
βgal
SST
F'
G'
H
PV;βgal/βgal (P14)
0.6
0.4
0.2
0.0
L1
L6
I
PV;βgal/PV (P14)
0.6
0.4
0.2
0.0
L1
L6
J
PV
RA
responding
SST
MGE-derived
CGE-derived
GABAergic neurons in the PFC

Fig.3

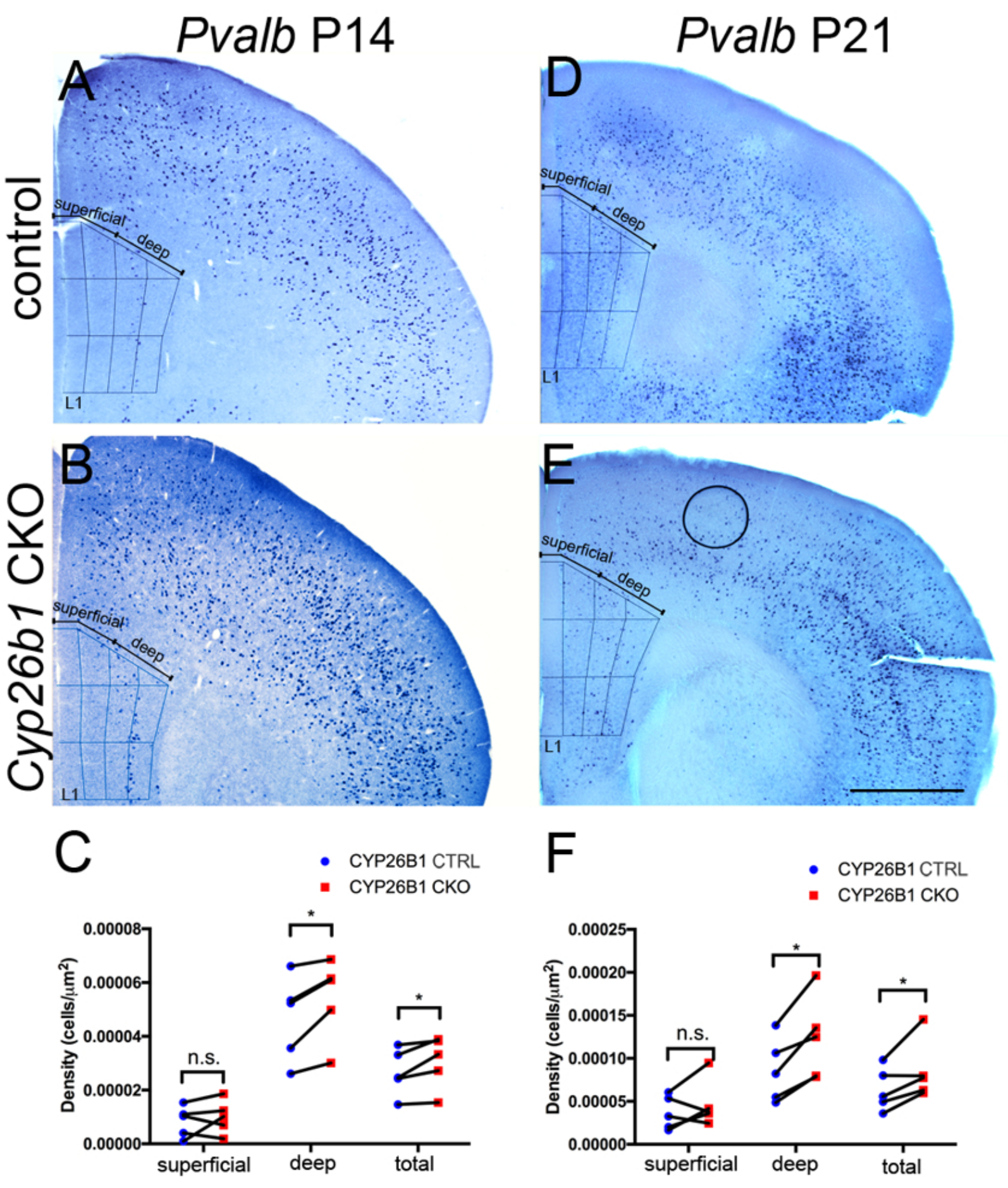
Pvalb P14
Pvalb P21
A
B
C
D
E
F
control
Cyp26b1 CKO
superficial
deep
L1
CYP26B1 CTRL
CYP26B1 CKO
Density (cells/μm²)
0.00008
0.00006
0.00004
0.00002
0.00000
0.00025
0.00020
0.00015
0.00010
0.00005
0.00000
n.s.
*
superficial
deep
total

Fig.4

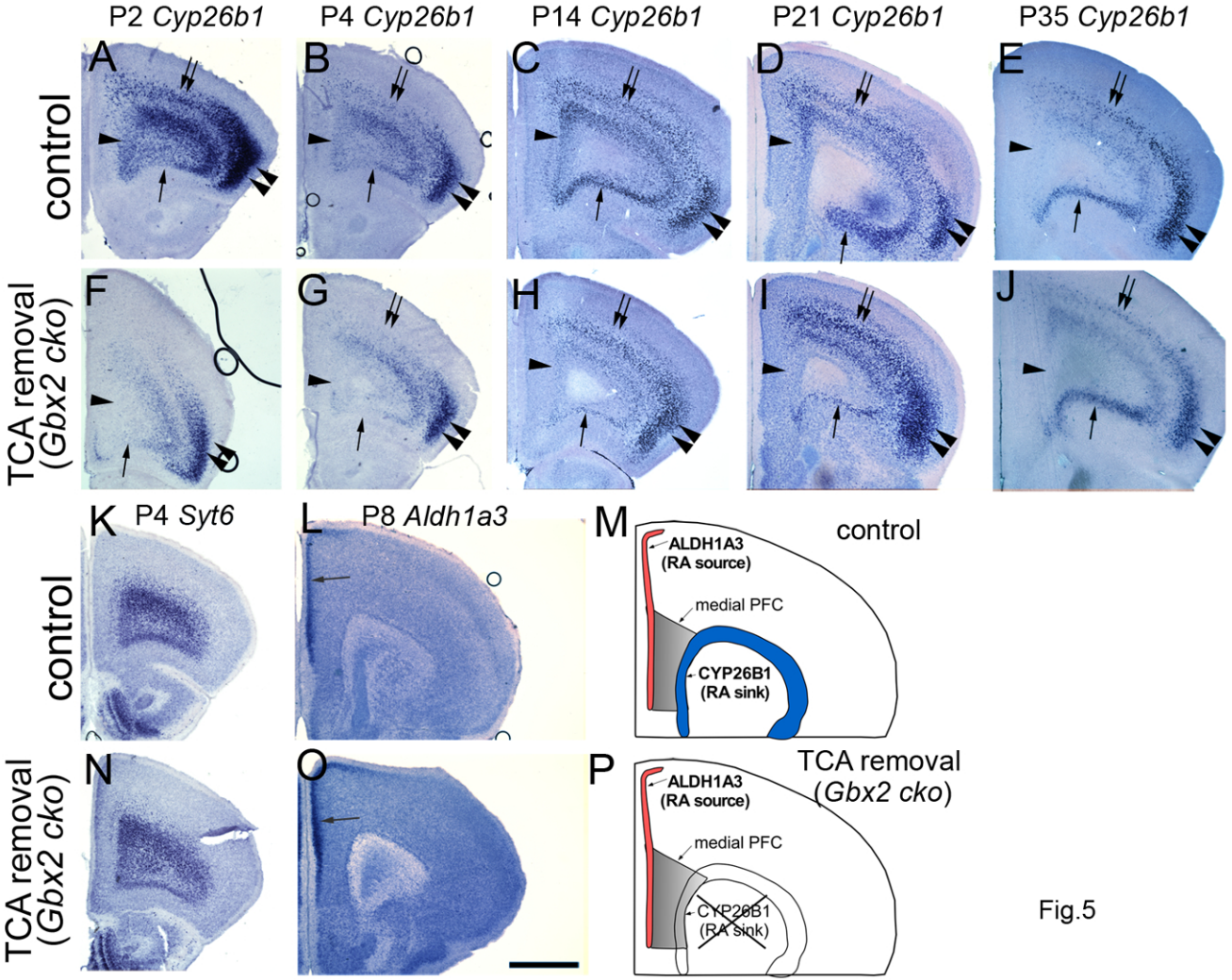
P2 Cyp26b1
P4 Cyp26b1
P14 Cyp26b1
P21 Cyp26b1
P35 Cyp26b1
A
B
C
D
E
control
F
G
H
I
J
TCA removal (Gbx2 cko)
K
P4 Syt6
L
P8 Aldh1a3
M
control
ALDH1A3 (RA source)
medial PFC
CYP26B1 (RA sink)
N
O
P
TCA removal (Gbx2 cko)
ALDH1A3 (RA source)
medial PFC
CYP26B1 (RA sink)

Fig.5

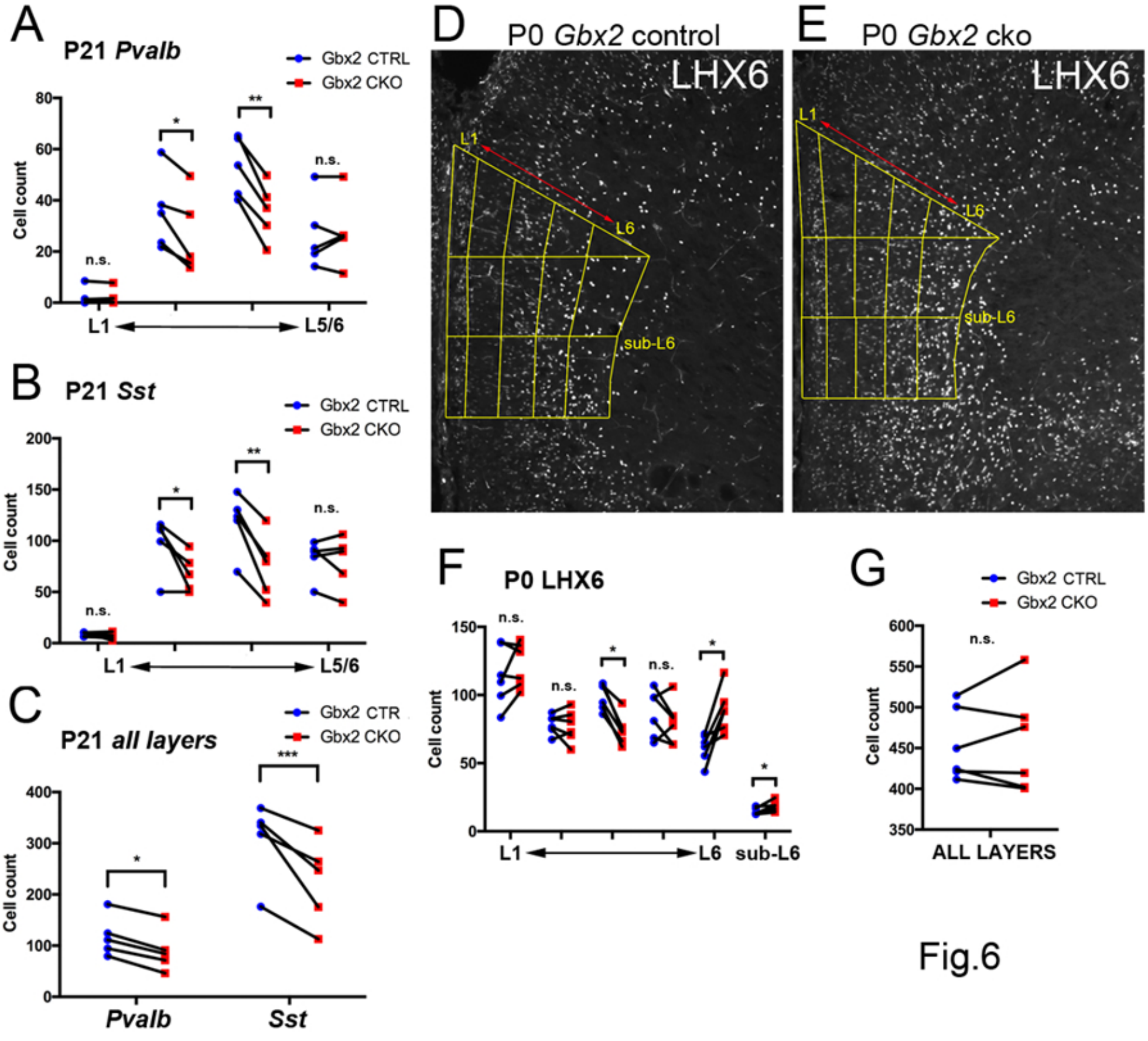
A
P21 Pvalb
Gbx2 CTRL
Gbx2 CKO
Cell count
80
60
40
20
0
n.s.
*
**
n.s.
L1
L5/6
B
P21 Sst
Gbx2 CTRL
Gbx2 CKO
Cell count
200
150
100
50
0
n.s.
*
**
n.s.
L1
L5/6
C
P21 all layers
Gbx2 CTR
Gbx2 CKO
Cell count
400
300
200
100
0
*
***
Pvalb
Sst
D
P0 Gbx2 control
LHX6
L1
L6
sub-L6
E
P0 Gbx2 cko
LHX6
L1
L6
sub-L6
F
P0 LHX6
Cell count
150
100
50
0
n.s.
n.s.
*
n.s.
*
*
L1
L6
sub-L6
G
Gbx2 CTRL
Gbx2 CKO
Cell count
600
550
500
450
400
350
n.s.
ALL LAYERS

Fig.6

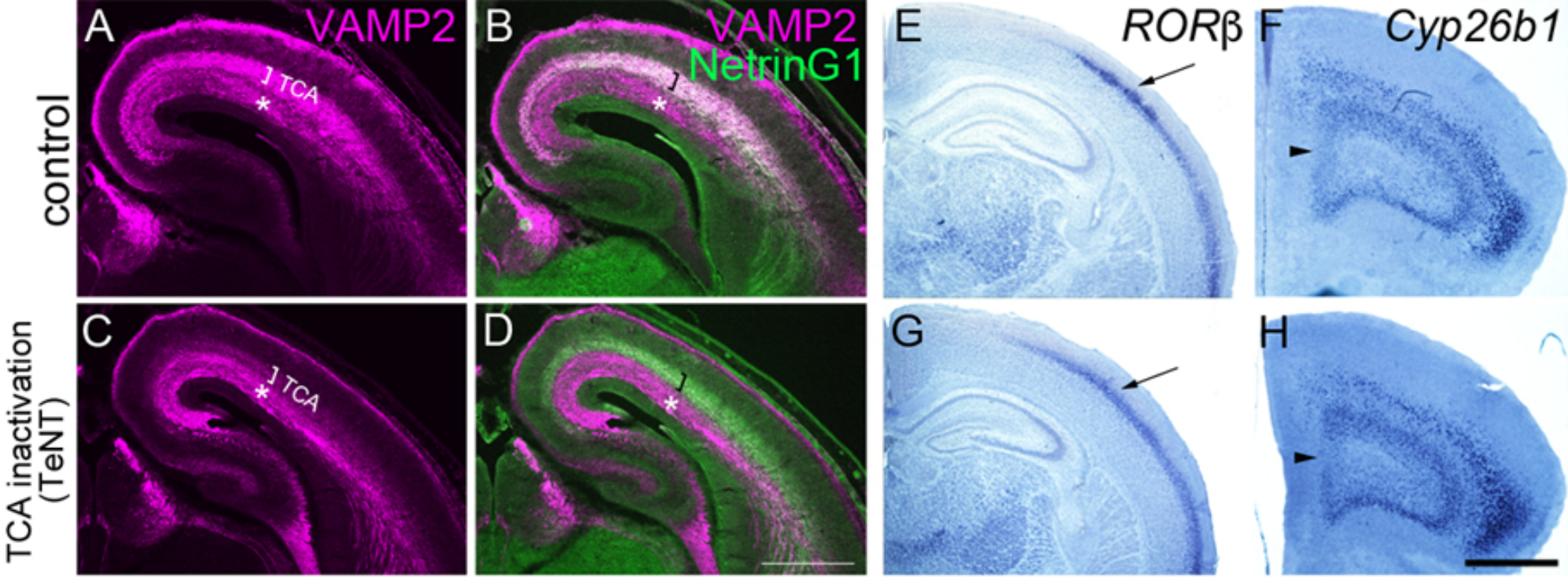
A
VAMP2
TCA
B
VAMP2
NetrinG1
C
TCA
D
E
RORβ
F
Cyp26b1
G
H
control
TCA inactivation
(TeNT)

Fig.7

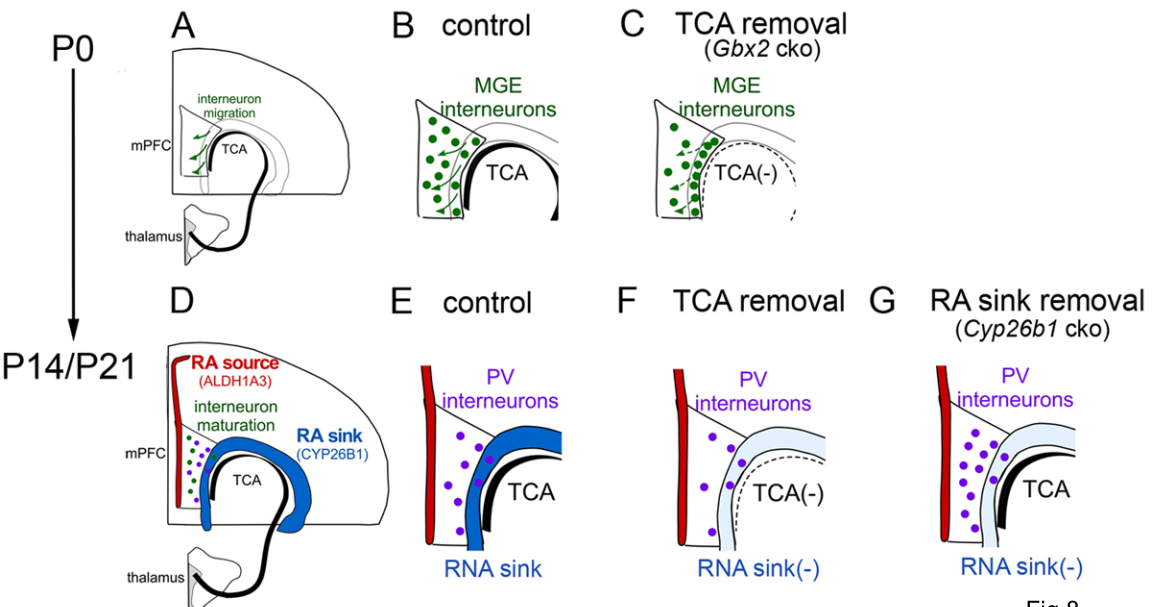
P0
P14/P21
A
interneuron migration
mPFC
TCA
thalamus
B control
MGE interneurons
TCA
C TCA removal
(Gbx2 cko)
MGE interneurons
TCA(-)
D
RA source
(ALDH1A3)
interneuron maturation
RA sink
(CYP26B1)
mPFC
TCA
thalamus
E control
PV interneurons
TCA
RNA sink
F TCA removal
PV interneurons
TCA(-)
RNA sink(-)
G RA sink removal
(Cyp26b1 cko)
PV interneurons
TCA
RNA sink(-)

Fig.8